CHAPTER 9 □ DIFFUSION APPROXIMATION

In Chapter 8 we discussed approximate single scattering and first order solutions applicable to a tenuous medium. In general, they are valid only when the volume density, which is the ratio of the volume occupied by particles to the total volume of the medium, is considerably smaller than 0.1%. When the volume density is much greater than 1%, the diffusion approximation gives relatively simple and good solutions. For a volume density in the neighborhood of 1%, neither the first order solution nor the diffuse approximation may be valid, and the complete equation of transfer must be solved. In this chapter we discuss the derivation of the diffusion equation from the equation of transfer together with some solutions for a parallel-plane problem. The diffusion approximation has been successfully used in the analysis of the optical fiber oximeter of blood (Johnson, 1970; Johnson and Guy, 1972; Reynolds *et al.*, 1976).

9-1 DERIVATION OF THE DIFFUSION EQUATION

As was discussed in Section 7-4, the intensity in a random medium can be divided into two parts: the reduced incident intensity I_{ri} and the diffuse intensity I_d. For a given incident wave, I_{ri} can be easily calculated. The diffuse intensity, however, must satisfy the equation of transfer [see Eq. (7-30)]:

$$\frac{dI_d(\mathbf{r}, \hat{\mathbf{s}})}{ds} = -\rho\sigma_t I_d(\mathbf{r}, \hat{\mathbf{s}}) + \frac{\rho\sigma_t}{4\pi}\int_{4\pi} p(\hat{\mathbf{s}}, \hat{\mathbf{s}}')I_d(\mathbf{r}, \hat{\mathbf{s}}')\, d\omega' + \varepsilon_{ri}(\mathbf{r}, \hat{\mathbf{s}}) + \varepsilon(\mathbf{r}, \hat{\mathbf{s}}) \quad (9\text{-}1)$$

where ε_{ri} is the equivalent source function due to the reduced incident intensity I_{ri}:

$$\varepsilon_{ri}(\mathbf{r}, \hat{\mathbf{s}}) = \frac{\rho\sigma_t}{4\pi}\int_{4\pi} p(\hat{\mathbf{s}}, \hat{\mathbf{s}}')I_{ri}(\mathbf{r}, \hat{\mathbf{s}}')\, d\omega' \quad (9\text{-}2)$$

and $\varepsilon(\mathbf{r}, \hat{\mathbf{s}})$ is the source function.

For more on diffusion approximation, see Bell and Glasstone (1970, Chapter 3) and Morse and Feshback (1953, Section 2.4).

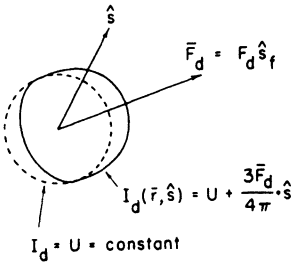

FIG. 9-1 Diffuse intensity $I_d(\mathbf{r}, \hat{\mathbf{s}})$ for diffusion approximation.

In the diffusion approximation we assume that the diffuse intensity encounters many particles and is scattered almost uniformly in all directions, and therefore its angular distribution is almost uniform (see Fig. 9-1). The angular dependence cannot be constant, however, because if it were constant, the flux $\mathbf{F}_d$ would be zero, and there would be no net power propagation. The diffuse intensity should therefore have slightly more magnitude in the direction of the net flux flow than in the backward direction. Mathematically we describe this situation by assuming that $I_d(\mathbf{r}, \hat{\mathbf{s}})$ is approximated by

$$I_d(\mathbf{r}, \hat{\mathbf{s}}) \simeq U_d(\mathbf{r}) + c\mathbf{F}_d(\mathbf{r}) \cdot \hat{\mathbf{s}} \tag{9-3}$$

where c is a constant, the diffuse flux vector $\mathbf{F}_d(\mathbf{r})$, whose direction is given by a unit vector $\hat{\mathbf{s}}_f$, is expressed by

$$\mathbf{F}_d(\mathbf{r}) = \int_{4\pi} I_d(\mathbf{r}, \hat{\mathbf{s}})\hat{\mathbf{s}}\, d\omega = F_d(\mathbf{r})\hat{\mathbf{s}}_f \tag{9-4}$$

and $U_d(\mathbf{r})$ is the average diffuse intensity, which is proportional to the energy density [see Eq. (7-7)],

$$U_d(\mathbf{r}) = \frac{1}{4\pi}\int_{4\pi} I_d(\mathbf{r}, \hat{\mathbf{s}})\, d\omega. \tag{9-5}$$

$I_d(\mathbf{r}, \hat{\mathbf{s}})$ as given by (9-3) is pictured in Fig. 9-1. The constant c in (9-3) can be easily found by noting that

$$F_d(\mathbf{r}) = \mathbf{F}_d(\mathbf{r}) \cdot \hat{\mathbf{s}}_f = \int_{4\pi} I_d(\mathbf{r}, \hat{\mathbf{s}})\hat{\mathbf{s}} \cdot \hat{\mathbf{s}}_f\, d\omega. \tag{9-6}$$

Substituting (9-3) into (9-6), we get $c = 3/4\pi$, and therefore the diffusion approximation of the diffuse intensity is given by

$$I_d(\mathbf{r}, \hat{\mathbf{s}}) = U_d(\mathbf{r}) + (3/4\pi)\mathbf{F}_d(\mathbf{r}) \cdot \hat{\mathbf{s}}. \tag{9-7}$$

Equation (9-7) may be regarded as the first two terms of a Taylor's expansion of I_d in terms of the powers of $\hat{\mathbf{s}} \cdot \hat{\mathbf{s}}_f$, and therefore the second term of (9-7) must be considerably smaller than the first: $U_d \gg |\mathbf{F}_d|$.

We now proceed to derive a diffusion equation based on the approximation (9-7). First, we integrate (9-1) over all 4π of solid angle and obtain a general power relationship [see (7-28a)]

$$\operatorname{div} \mathbf{F}_d(\mathbf{r}) = -4\pi\rho\sigma_a U_d(\mathbf{r}) + 4\pi\rho\sigma_s U_{ri} + E(\mathbf{r}) \tag{9-8}$$

where $U_{ri}(\mathbf{r}) = (1/4\pi)\int_{4\pi} I_{ri}(\mathbf{r}, \hat{\mathbf{s}})\, d\omega$ and $E(\mathbf{r}) = \int_{4\pi} \varepsilon(\mathbf{r}, \hat{\mathbf{s}})\, d\omega$. Next, we substitute (9-7) into (9-1). Under the assumption that the phase function $p(\hat{\mathbf{s}}, \hat{\mathbf{s}}')$ is a function of the angle between $\hat{\mathbf{s}}$ and $\hat{\mathbf{s}}'$, we obtain

$$\hat{\mathbf{s}} \cdot \operatorname{grad} U_d + \frac{3}{4\pi}\hat{\mathbf{s}} \cdot \operatorname{grad}(\mathbf{F}_d \cdot \hat{\mathbf{s}})$$

$$= -\rho\sigma_t U_d - \frac{3}{4\pi}\rho\sigma_t \mathbf{F}_d \cdot \hat{\mathbf{s}} + \rho\sigma_s U_d + \frac{3}{4\pi}\rho\sigma_t \mathbf{F}_d \cdot \hat{\mathbf{s}} p_1 + \varepsilon_{ri} + \varepsilon \tag{9-9}$$

where ε is defined in (9-1), and p_1 is given by

$$p_1 = \frac{1}{4\pi}\int_{4\pi} p(\hat{\mathbf{s}}, \hat{\mathbf{s}}')\hat{\mathbf{s}} \cdot \hat{\mathbf{s}}'\, d\omega', \tag{9-10}$$

and it represents the averaged forward scattering ($\hat{\mathbf{s}} \cdot \hat{\mathbf{s}}' > 0$) minus the backward scattering ($\hat{\mathbf{s}} \cdot \hat{\mathbf{s}}' < 0$) of a single particle.

It is often convenient to write $p_1 = W_0\,\bar{\mu}$ where W_0 is the albedo of a single particle and $\bar{\mu}$ is the mean cosine of the scattering angle θ given by

$$\bar{\mu} = \left(\int_{4\pi} p(\hat{\mathbf{s}}, \hat{\mathbf{s}}')\mu\, d\omega'\right) \Big/ \left(\int_{4\pi} p(\hat{\mathbf{s}}, \hat{\mathbf{s}}')\, d\omega'\right) \tag{9-11}$$

where $\mu = \cos\theta = \hat{\mathbf{s}} \cdot \hat{\mathbf{s}}'$. We note that since the phase function $p(\hat{\mathbf{s}}, \hat{\mathbf{s}}')$ is a function of the scattering angle γ only, we can expand the phase function in a series of Legendre functions:

$$p(\hat{\mathbf{s}}, \hat{\mathbf{s}}') = \sum_{n=0}^{\infty} W_n P_n(\cos\gamma), \qquad \cos\gamma = \hat{\mathbf{s}} \cdot \hat{\mathbf{s}}' \tag{9-12a}$$

and p_1 is given by

$$p_1 = W_1/3, \qquad \bar{\mu} = p_1/W_0 = W_1/3W_0. \tag{9-12b}$$

The phase function can often be approximated by the following form involving only W_0 and $\bar{\mu}$:

$$p(\mu) = W_0(1 - \bar{\mu}^2)[1 + \bar{\mu}^2 - 2\bar{\mu}\mu]^{-3/2}. \tag{9-12c}$$

This is called the Henyey–Greenstein formula and is often used to describe scattering from blood cells (Reynolds, 1975) and clouds (Danielson *et al.*, 1969; Henyey and Greenstein, 1941).

Now we multiply (9-9) by $\hat{\mathbf{s}}$ and integrate over all 4π, and obtain†

$$\text{grad } U_d = -\frac{3}{4\pi}\rho\sigma_t(1-p_1)\,\mathbf{F}_d + \frac{3}{4\pi}\int_{4\pi}\varepsilon_{ri}(\mathbf{r},\hat{\mathbf{s}})\hat{\mathbf{s}}\,d\omega + \frac{3}{4\pi}\int_{4\pi}\varepsilon(\mathbf{r},\hat{\mathbf{s}})\hat{\mathbf{s}}\,d\omega. \tag{9-13}$$

The quantity $\sigma_t(1-p_1)$ is called the transport cross section σ_{tr} (Bell and Glasstone, 1970, p. 104). It indicates that if the scattering is anisotropic, the equivalent total cross section is reduced by the factor $1-p_1$ from the isotropic case. The transport cross section is also written as

$$\sigma_{tr} = \sigma_t(1-p_1) = \sigma_s(1-\bar{\mu}) + \sigma_a. \tag{9-14}$$

As indicated in (3-33), if the particle density is increased, the equivalent scattering cross section is decreased by the factor $1-H$ where H is the ratio of the volume occupied by scatterers to the total volume. In terms of the number density ρ and the volume V_e of a single scatterer, H is equal to ρV_e:

$$\sigma_s \to \sigma_s(1-H). \tag{9-15a}$$

The transport cross section σ_{tr} for a high density medium should then be given by

$$\sigma_{tr} \to \sigma_s(1-H)(1-\bar{\mu}) + \sigma_a. \tag{9-15b}$$

Equation (9-8) gives div $\mathbf{F}_d$ in terms of U_d and (9-13) gives grad U_d in terms of $\mathbf{F}_d$. We eliminate $\mathbf{F}_d$ from these two equations by taking $\mathbf{F}_d$ from (9-13), substituting it into (9-8), and obtain a differential equation for U_d:

$$\nabla^2 U_d(\mathbf{r}) - \kappa_d{}^2 U_d(\mathbf{r}) = -3\rho\sigma_s\rho\sigma_{tr}\,U_{ri}(\mathbf{r}) - \frac{3}{4\pi}\rho\sigma_{tr}\,E(\mathbf{r}) + \frac{3}{4\pi}\nabla\cdot\int_{4\pi}\varepsilon_{ri}(\mathbf{r},\hat{\mathbf{s}})\hat{\mathbf{s}}\,d\omega + \frac{3}{4\pi}\nabla\cdot\int_{4\pi}\varepsilon(\mathbf{r},\hat{\mathbf{s}})\hat{\mathbf{s}}\,d\omega \tag{9-16}$$

where $\kappa_d{}^2 = 3\rho\sigma_a\rho\sigma_{tr}$. It is understood that for a high density medium, σ_s and σ_{tr} in (9-16) should be given by (9-15a) and (9-15b). Equation (9-16) is the fundamental steady state diffusion equation‡ for the average diffuse intensity $U_d(\mathbf{r})$, and together with the boundary condition discussed in the following section, constitutes the complete mathematical description of the diffusion approximation. Once the diffusion intensity is found, the flux $\mathbf{F}_d$ can be calculated from (9-13).

† For any vector $\mathbf{A}$, $\int_{4\pi}\hat{\mathbf{s}}(\hat{\mathbf{s}}\cdot\mathbf{A})\,d\omega = 4\pi\mathbf{A}/3$, and $\int_{4\pi}\hat{\mathbf{s}}[\hat{\mathbf{s}}\cdot\text{grad}(\mathbf{A}\cdot\hat{\mathbf{s}})]\,d\omega = 0$.

‡ A time-varying diffusion equation is of the form $D\nabla^2 u - au = \partial u/\partial t$, where D is the diffusion coefficient and a represents absorption (see Morse and Feshbach, 1953, Section 2.4).

9-2 BOUNDARY CONDITIONS

The exact boundary condition for the diffuse intensity I_d is that at the surface there should be no diffuse intensity entering the medium from outside [see (7-32)]:

$$I_d(\mathbf{r}, \hat{\mathbf{s}}) = 0 \quad \text{when } \hat{\mathbf{s}} \text{ is pointed inward.} \tag{9-17}$$

According to the diffusion approximation, however, $I_d(\mathbf{r}, \hat{\mathbf{s}})$ has a simple angular distribution given by (9-7), and the diffusion equation is given in terms of a single scalar function $U_d(\mathbf{r})$. Because of this approximate representation, the boundary condition (9-17) cannot be satisfied exactly, and some approximate boundary conditions must be considered. One such approximation is the condition at a surface that the total diffuse flux directed inward must be zero:

$$\int_{2\pi} I_d(\mathbf{r}, \hat{\mathbf{s}})(\hat{\mathbf{s}} \cdot \hat{\mathbf{n}})\, d\omega = 0 \tag{9-18}$$

where $\hat{\mathbf{n}}$ is a unit vector normally directed inward, and the integration is performed over 2π in the hemisphere $\hat{\mathbf{s}} \cdot \hat{\mathbf{n}} > 0$ (see Fig. 9-2).

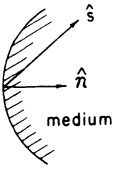

FIG. 9-2 Geometry showing the directions of $\hat{\mathbf{n}}$ and $\hat{\mathbf{s}}$ for the boundary condition (9-18).

The condition (9-18) can be expressed in terms of the average intensity U_d alone. To do this, we first write $\mathbf{F}_d$ as a sum of the component F_{dn} normal to and the component F_{dt} tangential to the surface:

$$\mathbf{F}_d = F_{dn}\hat{\mathbf{n}} + F_{dt}\hat{\mathbf{t}}. \tag{9-19}$$

Now we substitute (9-7) together with (9-19) into (9-18) and perform the integration using a spherical coordinate system with $\hat{\mathbf{z}} = \hat{\mathbf{n}}$ and $\hat{\mathbf{x}} = \hat{\mathbf{t}}$:

$$\int_{2\pi} (F_{dt}\hat{\mathbf{t}} \cdot \hat{\mathbf{s}})(\hat{\mathbf{s}} \cdot \hat{\mathbf{n}})\, d\omega = F_{dt} \int_0^{2\pi} \int_0^{\pi/2} \sin\theta \cos\phi \cos\theta \sin\theta\, d\theta\, d\phi = 0 \tag{9-20}$$

$$\int_{2n} (F_{dn}\hat{\mathbf{n}} \cdot \hat{\mathbf{s}})(\hat{\mathbf{s}} \cdot \hat{\mathbf{n}})\, d\omega = F_{dn} \int_0^{2\pi} \int_0^{\pi/2} \cos^2\theta \sin\theta\, d\theta\, d\phi = \frac{2\pi}{3} F_{dn}.$$

Then the boundary condition (9-18) becomes

$$\tfrac{1}{2}U_d(\mathbf{r}_s) + \frac{F_{dn}(\mathbf{r}_s)}{4\pi} = 0 \qquad \text{at the surface} \quad \mathbf{r} = \mathbf{r}_s. \tag{9-21}$$

Next we express F_{dn} in (9-21) in terms of U_d by using (9-13):

$$F_{dn} = \hat{\mathbf{n}} \cdot \mathbf{F}_d = -\frac{4\pi}{3\rho\sigma_{tr}} \hat{\mathbf{n}} \cdot \text{grad } U_d(\mathbf{r}) + \hat{\mathbf{n}} \cdot \mathbf{Q}_1(\mathbf{r}) \tag{9-22}$$

where

$$\mathbf{Q}_1(\mathbf{r}) = \frac{1}{\rho\sigma_{tr}} \int_{4\pi} [\varepsilon_{ri}(\mathbf{r}, \hat{\mathbf{s}}) + \varepsilon(\mathbf{r}, \hat{\mathbf{s}})]\hat{\mathbf{s}}\, d\omega.$$

In the absence of sources, $\varepsilon(\mathbf{r}, \hat{\mathbf{s}}) = 0$ and using (9-2), we write

$$\mathbf{Q}_1(\mathbf{r}) = \frac{\sigma_t}{\sigma_{tr}} \int_{4\pi} d\omega' \left[\frac{1}{4\pi} \int_{4\pi} p(\hat{\mathbf{s}}, \hat{\mathbf{s}}')\hat{\mathbf{s}}\, d\omega\right] I_{ri}(\mathbf{r}, \hat{\mathbf{s}}'). \tag{9-23}$$

Note that if the scatterers are isotropic, $p(\hat{\mathbf{s}}, \hat{\mathbf{s}}') = \text{const}$ and $\mathbf{Q}_1 = 0$. Therefore, $\mathbf{Q}_1$ represents the effect of anisotropy of the scattering pattern.

Substituting (9-22) into (9-21), we get the boundary condition in terms of U_d:

$$U_d(\mathbf{r}_s) - \frac{2}{3\rho\sigma_{tr}} \frac{\partial}{\partial n} U_d(\mathbf{r}_s) + \frac{2\hat{\mathbf{n}} \cdot \mathbf{Q}_1(\mathbf{r}_s)}{4\pi} = 0 \tag{9-24}$$

where $\partial/\partial n$ is the normal derivative in the direction toward the medium.

It should be emphasized that the boundary condition (9-24) is only approximate. In fact, it is known that the diffusion approximation itself holds only for the region far from the boundary and the source. We can get some idea of how approximate (9-24) may be by comparing it with an exact boundary condition for a special case. The problem of isotropic scatterers provides such a comparison because it is possible to obtain an exact solution for a semi-infinite slab containing isotropic scatterers. This is called the Milne problem, the exact solution of which can be divided into a part that satisfies the diffusion equation and another part (see Sections 12-2 and 12-6). The diffusion part itself satisfies the boundary condition

$$U_d(\mathbf{r}_s) - \frac{0.7104}{\rho\sigma_t W_0} \frac{\partial}{\partial n} U_d(\mathbf{r}_s) = 0 \tag{9-25}$$

valid within 0.7% when the albedo $W_0 = \sigma_s/\sigma_t$ is in the range $0.6 \leq W_0 \leq 1$. We note that $\mathbf{Q}_1 = 0$ and the constant $2/3\rho\sigma_{tr}$ in (9-24) reduces to $2/3\rho\sigma_t$ for isotropic scatterers, and this constant should be compared with $0.7104/\rho\sigma_t W_0$ in (9-25). It is clear then that $\frac{2}{3}$ in (9-24) should be considered only approximate and that the diffusion solution should be valid only when the albedo W_0 is close to unity and the particles are mostly scattering rather than absorbing.

9-3 COLLIMATED BEAM INCIDENT UPON A SLAB OF PARTICLES

As an example of the diffusion solution, we consider a collimated beam incident normally upon a slab containing random particles (see Fig. 9-3).

First, we examine the diffusion equation (9-16). The reduced incident intensity for the collimated beam shown in Fig. 9-3 is given by (see Section 8-3)

$$I_{ri}(\mathbf{r}, \hat{\mathbf{s}}) = F_0(\boldsymbol{\rho}) \exp(-\rho\sigma_t z)\, \delta(\hat{\boldsymbol{\omega}} - \hat{\boldsymbol{\omega}}_z) \tag{9-26}$$

where $F_0(\boldsymbol{\rho})$ is the flux density [see (7-33)], $\boldsymbol{\rho} = x\hat{\mathbf{x}} + y\hat{\mathbf{y}}$, $\hat{\boldsymbol{\omega}}$ and $\hat{\boldsymbol{\omega}}_z$ are the unit vectors pointed in the $\hat{\mathbf{s}}$ and $\hat{\mathbf{z}}$ direction, respectively, and $\delta(\hat{\boldsymbol{\omega}} - \hat{\boldsymbol{\omega}}_z)$ is a solid angle delta function. There is no other source present in the medium. Therefore, $E(\mathbf{r}) = 0$ and $\varepsilon(\mathbf{r}, \hat{\mathbf{s}}) = 0$. Substituting (9-26) into (9-2) and (9-8), the source terms on the right-hand side of (9-16) can be expressed in terms of F_0. We note that

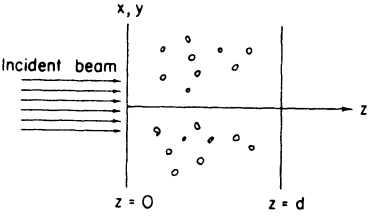

FIG. 9-3 Collimated beam incident upon a slab containing randomly distributed scatterers.

$$\begin{aligned} U_{ri}(\mathbf{r}) &= \frac{F_0(\boldsymbol{\rho})}{4\pi} \exp(-\rho\sigma_t z) \\ \nabla \cdot \int_{4\pi} \varepsilon_{ri}(\mathbf{r}, \hat{\mathbf{s}})\hat{\mathbf{s}}\, d\omega &= \left[\frac{\rho\sigma_t}{4\pi} \int_{4\pi} p(\hat{\mathbf{s}}, \hat{\mathbf{z}})\hat{\mathbf{s}}\, d\omega\right] \cdot \nabla[F_0(\boldsymbol{\rho}) \exp(-\rho\sigma_t z)] \\ &= -(\rho\sigma_t)^2 p_1 F_0(\boldsymbol{\rho}) \exp(-\rho\sigma_t z) \end{aligned} \tag{9-27}$$

where it is noted that the integral $\int p(\hat{\mathbf{s}}, \hat{\mathbf{z}})\hat{\mathbf{s}}\, d\omega$ is pointed in the z direction.

Substituting (9-27) into (9-16), we get the following diffusion equation applicable to the case of a collimated incident beam:

$$\begin{aligned} &\nabla^2 U_d(\mathbf{r}) - \kappa_d{}^2 U_d(\mathbf{r}) = -Q(\mathbf{r}), \qquad \kappa_d{}^2 = 3(\rho\sigma_a)(\rho\sigma_{tr}) \\ &Q(\mathbf{r}) = [3\rho\sigma_s \rho\sigma_{tr} + 3\rho\sigma_s \rho\sigma_t \bar{\mu}] \frac{F_0(\boldsymbol{\rho})}{4\pi} \exp(-\rho\sigma_t z). \end{aligned} \tag{9-28}$$

The boundary conditions for the slab shown in Fig. 9-3 are given by (9-24), which we write in the form

$$\begin{aligned} U_d(\mathbf{r}) - h\frac{\partial}{\partial z}U_d(\mathbf{r}) + \frac{Q_1(\mathbf{r})}{2\pi} = 0 \qquad &\text{at} \quad z = 0 \\ U_d(\mathbf{r}) + h\frac{\partial}{\partial z}U_d(\mathbf{r}) - \frac{Q_1(\mathbf{r})}{2\pi} = 0 \qquad &\text{at} \quad z = d \end{aligned} \tag{9-29}$$

where $h = 2/3\rho\sigma_{tr}$ and $Q_1(\mathbf{r}) = (\sigma_s\bar{\mu}/\sigma_{tr})F_0(\boldsymbol{\rho})\exp(-\rho\sigma_t z)$.

Once the diffuse average intensity $U_d(\mathbf{r})$ is found, the flux and the diffuse intensity can be found from (9-13) and (9-7):

$$\mathbf{F}_d(\mathbf{r}) = \frac{\sigma_s\bar{\mu}F_0(\boldsymbol{\rho})}{\sigma_{tr}}\exp(-\rho\sigma_t z)\hat{\mathbf{z}} - \frac{4\pi}{3\rho\sigma_{tr}}\operatorname{grad} U_d(\mathbf{r}). \tag{9-30}$$

For a high density medium, σ_s and σ_{tr} in (9-28)–(9-30) must be replaced by those in (9-15a) and (9-15b).

9-4 SOLUTION FOR A PLANE WAVE INCIDENT UPON A SLAB OF PARTICLES

The case of a plane wave incident upon a slab can be analyzed by the formulation given in the preceding section. For a plane wave, $F_0(\boldsymbol{\rho})$ in (9-26) becomes constant F_0 and (9-28) becomes

$$\frac{\partial^2}{\partial z^2}U_d(z) - \kappa_d^2 U_d(z) = -Q_0\exp(-\rho\sigma_t z) \tag{9-31}$$

where $Q_0 = [3\rho\sigma_s\rho\sigma_{tr} + 3\rho\sigma_s\rho\sigma_t\bar{\mu}](F_0/4\pi)$. The boundary conditions (9-29) are

$$\begin{aligned} U_d(z) - h\frac{\partial}{\partial z}U_d(z) + \frac{Q_1(z)}{2\pi} = 0 \qquad &\text{at} \quad z = 0 \\ U_d(z) + h\frac{\partial}{\partial z}U_d(z) - \frac{Q_1(z)}{2\pi} = 0 \qquad &\text{at} \quad z = d \end{aligned} \tag{9-32}$$

where $Q_1(z) = (\sigma_s\bar{\mu}/\sigma_{tr})F_0\exp(-\rho\sigma_t z)$ and $h = 2/3\rho\sigma_{tr}$. The general solution of (9-31) is the sum of a particular solution U_{dp} and a complementary solution U_{dc}. To find a particular solution, we let

$$U_{dp}(z) = A\exp(-\rho\sigma_t z). \tag{9-33}$$

Substituting (9-33) into (9-31), we obtain

$$A = -Q_0/[(\rho\sigma_t)^2 - \kappa_d^2]. \tag{9-34}$$

The complementary solution U_{dc} satisfies

$$\frac{\partial^2}{\partial z^2} U_{dc} - \kappa_d^2 U_{dc} = 0 \tag{9-35}$$

and therefore we have

$$U_{dc}(z) = C_1 \exp(\kappa_d z) + C_2 \exp(-\kappa_d z). \tag{9-36}$$

C_1 and C_2 are unknown constants and are determined by applying the boundary conditions (9-32). Substituting $U_d(z) = U_{dp}(z) + U_{dc}(z)$ into (9-32) we get two equations for the two unknowns C_1 and C_2:

$$C_1(1 - \kappa_d h) + C_2(1 + \kappa_d h) = -A(1 + \rho\sigma_t h) - \frac{Q_1(0)}{2\pi}$$

$$C_1(1 + \kappa_d h)\exp(\kappa_d d) + C_2(1 - \kappa_d h)\exp(-\kappa_d d) \tag{9-37}$$

$$= -A(1 - \rho\sigma_t h)\exp(-\rho\sigma_t d) + \frac{Q_1(0)}{2\pi}\exp(-\rho\sigma_t d).$$

From these, we can easily determine C_1 and C_2.

It can be shown that for the case of a semi-infinite medium ($d \to \infty$), we have

$$C_1 \to 0, \qquad C_2 \to -\frac{A(1 + \rho\sigma_t h)}{(1 + \kappa_d h)} - \frac{Q_1(0)}{2\pi(1 + \kappa_d h)} \tag{9-38}$$

$$U_d(z) = A \exp(-\rho\sigma_t z) + C_2 \exp(-\kappa_d z).$$

The flux $\mathbf{F}_d(z)$ can be calculated from (9-30). Furthermore, if the scatterers are lossless, we have $\sigma_a \to 0$, and therefore we obtain

$$\mathbf{F}_d(z) = -F_0 \exp(-\rho\sigma_t z)\,\hat{\mathbf{z}}. \tag{9-39}$$

This shows that in a semi-infinite lossless medium, the diffuse flux $\mathbf{F}_d$ is equal in magnitude and opposite in direction to the reduced incident flux $\mathbf{F}_{ri}(z) = F_0 \exp(-\rho\sigma_t z)\hat{\mathbf{z}}$. Physically, this means that the incident flux F_0 is diffused throughout the medium, but eventually all the flux F_0 is scattered back and returned in the $-z$ direction.

For the totally lossless scatterers, $\kappa_d = 0$, and (9-35) becomes a Laplace equation:

$$(\partial^2/\partial z^2)U_{dc} = 0. \tag{9-40}$$

A solution should therefore be written as

$$U_{dc}(z) = C_1 z + C_2 \tag{9-41}$$

instead of (9-36). Applying the boundary conditions (9-32), we can easily obtain the solution for lossless scatterers.

9-5 SOLUTION FOR A COLLIMATED BEAM OF A FINITE WIDTH INCIDENT UPON A SLAB OF PARTICLES

A general solution of (9-28) and (9-29) can be obtained by using a Green's function $G(\mathbf{r}, \mathbf{r}')$ satisfying

$$\begin{aligned} &\nabla^2 G(\mathbf{r}, \mathbf{r}') - \kappa_d{}^2 G(\mathbf{r}, \mathbf{r}') = -\delta(\mathbf{r}, \mathbf{r}') \\ &G(\mathbf{r}, \mathbf{r}') - h \frac{\partial}{\partial z} G(\mathbf{r}, \mathbf{r}') = 0 \qquad \text{at} \quad z = 0 \\ &G(\mathbf{r}, \mathbf{r}') + h \frac{\partial}{\partial z} G(\mathbf{r}, \mathbf{r}') = 0 \qquad \text{at} \quad z = d. \end{aligned} \tag{9-42}$$

Using Green's second identity

$$\int [u\nabla^2 v - v\nabla^2 u]\, dV = \int \left[u \frac{\partial v}{\partial n} - v \frac{\partial u}{\partial n}\right] da \tag{9-43}$$

where $\partial/\partial n$ is the derivative in the outward normal direction, we get the complete solution U_d:

$$U_d(\mathbf{r}) = \int_V G(\mathbf{r}, \mathbf{r}') Q(\mathbf{r}')\, dV' + \int_s \frac{G(\mathbf{r}, \mathbf{r}') Q_1(\mathbf{r}')}{2\pi h}\, da' \tag{9-44}$$

where V covers all the region with $0 \leq z \leq d$ and with x and y ranging from $-\infty$ to $+\infty$. The Green's function in the cylindrical coordinate system with $\mathbf{r}$ and $\mathbf{r}'$ expressed by (ρ, ϕ, z) and (ρ', ϕ', z') is (Magnus and Oberhettinger, 1954, p. 155)

$$G(\mathbf{r}, \mathbf{r}') = \sum_{m=-\infty}^{\infty} \sum_{n=1}^{\infty} \frac{\exp[\mathrm{im}(\phi - \phi')]}{2\pi} \frac{Z_n(z) Z_n(z')}{N_n{}^2} K_m(\lambda_n \rho) I_m(\lambda_n \rho') \tag{9-45}$$

for $\rho > \rho'$. For $\rho < \rho'$, ρ and ρ' should be exchanged in (9-45). K_m and I_m are modified Bessel functions (Jahnke *et al.*, 1960, p. 207). $Z_n(z)$ is an eigenfunction satisfying the boundary condition (9-42) and is given by

$$Z_n(z) = \sin(k_n z + \gamma_n) \tag{9-46}$$

where the eigenvalue k_n should satisfy

$$\tan k_n d = 2hk_n/[(hk_n)^2 - 1] \tag{9-47}$$

and γ_n is given by $\gamma_n = \tan^{-1}(hk_n)$. $N_n{}^2$ is the normalization factor given by

$$N_n{}^2 = \int_0^d [Z_n(z)]^2\, dz \tag{9-48}$$

and λ_n is related to k_n through

$$\lambda_n{}^2 = k_n{}^2 + \kappa_d{}^2. \tag{9-49}$$

We now substitute (9-45) into (9-44) and obtain the complete solution. If the collimated beam is symmetric about the z axis, then $F_0(\boldsymbol{\rho})$ becomes a function of the magnitude of $\boldsymbol{\rho}$ only, $F_0(\rho)$. In this case, U_d has no dependence on ϕ and therefore we have

$$U_d(\rho, z) = 2\pi \int_0^\infty \rho' \, d\rho' \int_0^d dz' \, G_0(\rho, z; \rho', z') Q(\rho', z') + \frac{1}{h} \int_0^\infty \rho' \, d\rho' \, G_0(\rho, z; \rho', 0) Q_1(\rho', 0) \tag{9-50}$$

where

$$G_0(\rho, z; \rho', z') = \sum_{n=1}^{\infty} \frac{Z_n(z) Z_n(z')}{2\pi N_n^2} K_0(\lambda_n \rho) I_0(\lambda_n \rho')$$

for $\rho > \rho'$. ρ and ρ' are exchanged when $\rho < \rho'$.

The solution outlined in this section has been used to determine the diffusion characteristics of whole blood (Johnson, 1970; Johnson and Guy, 1972; Reynolds *et al.*, 1976; for light reflection from blood, see Anderson and Sekelj, 1967). From this theory, a model of fiberoptic catheter used for the spectrophotometric measurement of oxygen content (oxygen saturation) in blood was developed and compared with catheter reflectance data on the physiological variations in blood of HbCO, HbO_2, and hematocrit. Excellent agreement was found between experiments and model, substantiating the theoretical approach described in this chapter (Reynolds, 1975).

9-6 DIFFUSION FROM A POINT SOURCE

Let us consider the diffusion of power from a point source located at the origin radiating the total power P_0 uniformly in all directions in an infinite space containing randomly distributed scatterers. The source is expressed by (7-35):

$$\varepsilon(\mathbf{r}, \hat{\mathbf{s}}) = (P_0/4\pi)\, \delta(\mathbf{r}). \tag{9-51}$$

The diffusion equation (9-16) becomes

$$\nabla^2 U_d(\mathbf{r}) - \kappa_d^2 U_d(\mathbf{r}) = -(3/4\pi)\rho\sigma_{tr} P_0 \, \delta(\mathbf{r}) \tag{9-52}$$

and the solution is given by

$$U_d(\mathbf{r}) = \frac{\exp(-\kappa_d r)}{4\pi r} \left[\frac{3}{4\pi} \rho\sigma_{tr} P_0\right] \tag{9-53}$$

$$\mathbf{F}_d(\mathbf{r}) = -\frac{\partial}{\partial r}\left[\frac{\exp(-\kappa_d r)}{4\pi r}\right] P_0 \hat{\mathbf{r}} = \left[\frac{\kappa_d}{4\pi r} + \frac{1}{4\pi r^2}\right] \exp(-\kappa_d r) P_0 \hat{\mathbf{r}}. \tag{9-54}$$

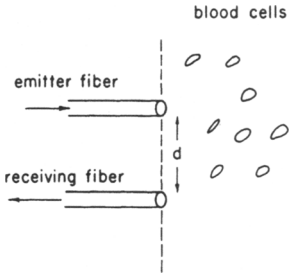

FIG. 9-4 Two-fiber reflectance measurement.

We note that in the case of lossless scatterers, $\kappa_d = 0$ and the total flux $4\pi r^2 F_d$ across the spherical surface at r is independent of r and equal to P_0 as demanded by the principle of the conservation of power.

9-7 TWO-FIBER REFLECTANCE

A two-fiber cuvette was constructed (Reynolds, 1975; also see Table 3-2 for characteristics of blood) to measure relative reflectance from a homogeneous medium of discrete scatterers to generate a fundamental set of

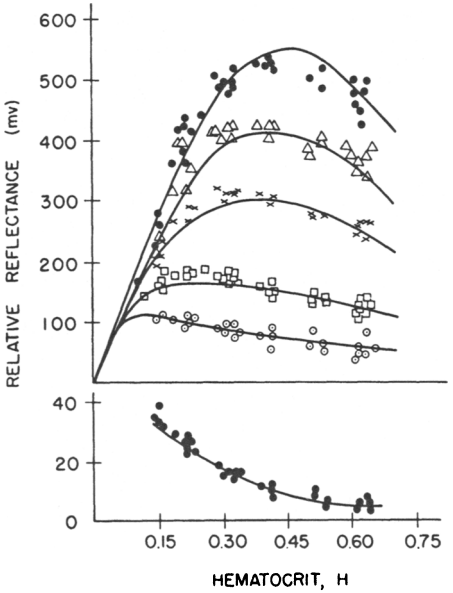

FIG. 9-5 Comparison of the theory and experimental results for reflectance from whole human blood versus hematocrit for six different fiber separation distances at a wavelength of $\lambda = 0.685$ μm and an oxygen saturation of 98.5%. Radial separation (mm): ● (upper), 0.54; △, 0.74; ×, 0.90; □, 1.27; ⊙, 1.66; ● (lower), 2.85.

reflectance data to verify the theory presented in Section 9-5 as a basis for the fiberoptic catheter model. The cuvette consists of two parallel optical fibers: a 0.508-mm-diameter emitter fiber which is normal to, in contact with, and fixed in relation to the scattering medium, and a 0.127-mm-diameter receiving fiber which is also in contact with the scattering medium and continuously adjustable to ± 5 mm in the radial direction about the center of the emitting fiber. Both emitting and receiving apertures remain in the same plane during measurements (Fig. 9-4).

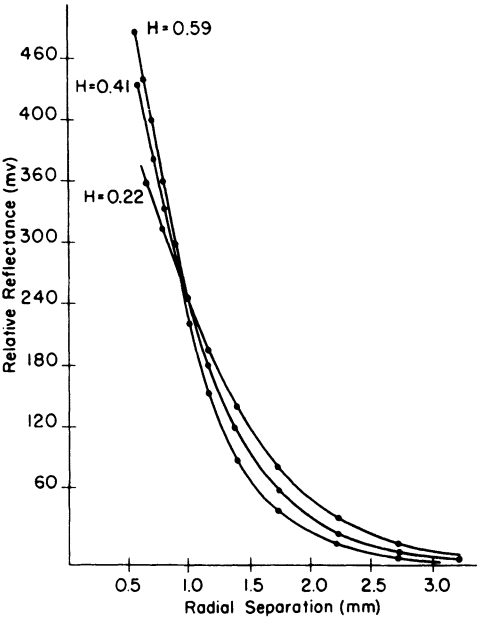

FIG. 9-6 Comparison of the diffusion theory and experimental results (●) for reflectance from whole human blood versus radial separation for three different hematocrits at a wavelength of $\lambda = 0.685$ μm and an oxygen saturation of 98.5%.

Figure 9-5 shows a comparison of the theoretical calculations based on the theory in Section 9-5 and the blood characteristics shown in Table 3-2 and the experimental data. Figure 9-6 shows that at a separation of about 0.9 mm, the reflectance is independent of a change in density between $H = 0.22$ and $H = 0.59$. This suggests that by fixing the fibers in a fiberoptic oximetry catheter at a specific separation distance, hematocrit variations could be removed from the oxygen saturation measurements.

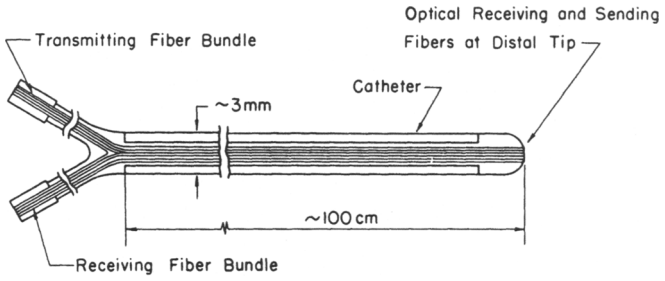

FIG. 9-7 Schematic of fiberoptic catheter.

9-8 THE FIBEROPTIC OXIMETER CATHETER

The fiberoptic catheter (Reynolds, 1975) illuminates blood by conveying light to the tip or distal end of the catheter by means of optical fibers (see Fig. 9-7). Light is backscattered by blood cells in the vicinity of the tip and transmitted by a second bundle of fibers to the proximal end for

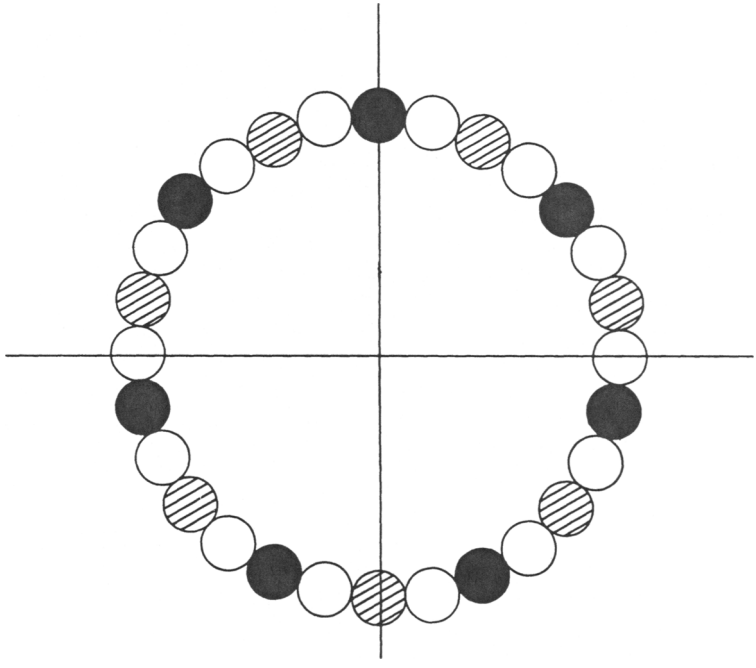

FIG. 9-8 Ring catheter configuration. ●, Sending fiber at 0.686 μm; ⊘, sending fiber at 0.925 μm; ○, receiving fiber.

evaluation by an oximeter to determine the oxygen saturation in the blood. A catheter fiber configuration such as the "ring" catheter shown in Fig. 9-8 consists of a consecutively interspaced set of optical fibers. One quarter of fibers transmits light at $\cong 0.9$ μm, another quarter transmits light at 0.68 μm, and the remaining one-half are used as receiving fibers. Measuring the ratio of the backscattered intensity at two wavelengths, one of which is more sensitive to oxygen saturation (0.6–0.7 μm) and the other of which is relatively insensitive to oxygen saturation (0.8–0.9 μm), cancels out variations such as pH and blood velocity which both affect the reflectance at both wavelengths in approximately an equal manner.

The motivation for constructing a fiberoptic catheter model is to develop a theoretical criterion for the design of the fiber configuration in the distal tip of a catheter to be used ultimately for the measurement of oxygen saturation in blood. Oxygen saturation (OS) is defined by the ratio of oxyhemoglobin to total hemoglobin. An empirically established relation for oxygen saturation in terms of the infrared reflectance R_i and the red reflectance R_r is given by

$$\mathrm{OS} = A - B\,R_i/R_r \tag{9-55}$$

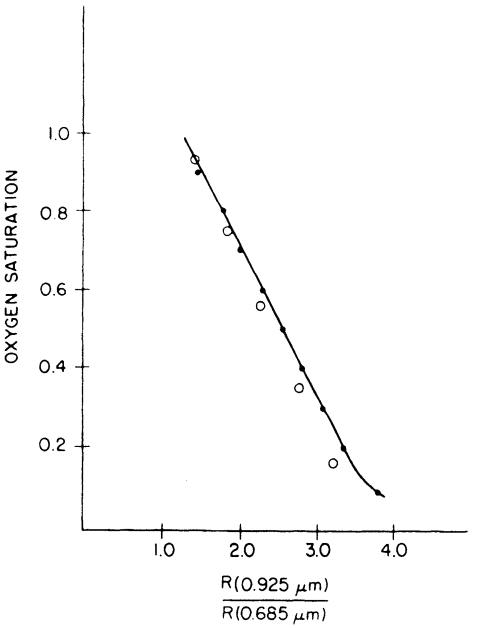

FIG. 9-9 Oxygen saturation versus ratio of reflectance at 0.925 μm to that at 0.685 μm for ring catheter model. ●, Diffusion theory; ○, data.

where R_i and R_r are backscattered intensities at 0.960 and 0.685 μm, respectively, and the constants A and B (functions of the geometry of the fiber bundle) and blood parameters can be empirically determined. Thus for different fiber configurations the constants A and B will differ and a calibration curve for each configuration is necessary for an accurate clinical verification of the *in vivo* operation of the fiberoptic oximeter. This calibration curve was in part the object of study of various researchers. Figure 9-9 shows both the experimental catheter calibration curve (data points) and the theoretically derived catheter model curve (solid line).